









# A New Set of Chisels for Galactic Archeology: Sc, V, and Zn as Taggers of Accreted Globular Clusters\*

A. Minelli<sup>1,2</sup> , A. Mucciarelli<sup>1,2</sup> , D. Massari<sup>2,3</sup> , M. Bellazzini<sup>2</sup> , D. Romano<sup>2</sup> , and F. R. Ferraro<sup>1,2</sup> 

<sup>1</sup>Dipartimento di Fisica e Astronomia *Augusto Righi*, Università degli Studi di Bologna, Via Gobetti 93/2, I-40129 Bologna, Italy

<sup>2</sup>INAF—Osservatorio di Astrofisica e Scienza dello Spazio di Bologna, Via Gobetti 93/3, I-40129 Bologna, Italy

<sup>3</sup>University of Groningen, Kapteyn Astronomical Institute, NL-9747 AD Groningen, The Netherlands

Received 2021 July 22; revised 2021 August 25; accepted 2021 August 25; published 2021 September 14

## Abstract

Chemical tagging is a powerful tool to reveal the origin of stars and globular clusters (GCs), especially when dynamics alone cannot provide robust answers. So far, mostly  $\alpha$ -elements and neutron capture elements have been used to distinguish stars born in the Milky Way (MW) from those born in external environments such as that of dwarf galaxies. Here, instead, we use iron-peak element abundances to investigate the origin of a sample of metal-rich GCs. By homogeneously analyzing high-resolution UVES spectra of giant stars belonging to four metal-rich GCs (namely NGC 5927, NGC 6388, NGC 6441, and NGC 6496), we find that while the  $\alpha$ -elements Si and Ca have similar abundance ratios for all four GCs, and Ti and neutron capture elements (La, Ba, and Eu) only show a marginal discrepancy, a stark difference is found when considering the abundances of some iron-peak elements (Sc, V, and Zn). In particular, NGC 6388 and NGC 6441 have abundance ratios for these iron-peak elements significantly lower (by  $\sim 0.5$  dex) than those measured in NGC 5927 and NGC 6496, which are clearly identified as born in situ MW clusters through an analysis of their orbital properties. These measurements indicate that the environment in which these clusters formed is different, and they provide robust evidence supporting an accreted origin from the same progenitor for NGC 6388 and NGC 6441.

*Unified Astronomy Thesaurus concepts:* [Stellar abundances \(1577\)](#); [Globular star clusters \(656\)](#)

## 1. Introduction

According to the generally accepted  $\Lambda$ -CDM cosmological model, large galaxies that we observe today were formed from the merging of small structures (White & Rees 1978; Helmi et al. 2018). The Milky Way (MW) is an excellent example of this assembly mechanism, since in the past it has experienced several merger events, many of which have been recently discovered thanks to the advent of the Gaia mission (e.g., Gaia-Enceladus-Sausage, Sequoia, and Thamnos; see Helmi 2020 for a comprehensive review). During this assembly process, the MW accreted both field stars and globular clusters (GCs). In particular, about 50%–60% of its current population of GCs has likely been accreted from different external progenitors, while the rest has likely formed in situ (Massari et al. 2019; Forbes 2020). So far, the accreted or in situ origin of the GCs has been primarily assessed by using their dynamics, coupled with information on their age–metallicity relation (Kruijssen et al. 2019; Massari et al. 2019). However, the dynamical properties of some GCs do not allow a clear-cut classification.

Chemical tagging (Freeman & Bland-Hawthorn 2002) is a powerful tool to reveal the origin of stars by means of their chemical patterns. In particular, it has been shown both theoretically (e.g., Matteucci & Brocato 1990) and observationally (e.g., Fernández-Alvar et al. 2018; Helmi et al. 2018), that abundance of  $\alpha$ -elements is an efficient tool to distinguish stars born in the MW from those born in dwarf galaxies. Furthermore, the slow neutron capture elements were observed to be enhanced in dwarf galaxies with respect to MW stars of similar metallicity (see, e.g., Tolstoy et al. 2009). Minelli et al. (2021) proposed to use the chemical abundance ratios of some iron-peak elements,

namely Sc, V, and Zn, as diagnostics to identify possible extragalactic stars in the metal-rich regime ( $[\text{Fe}/\text{H}] > -1$  dex). In a thorough and homogeneous comparison of chemical compositions between the Large Magellanic Cloud (LMC), the Sagittarius (Sgr) dwarf spheroidal, and the MW, they found that the largest difference between LMC/Sgr and MW stars occurs in  $[\text{V}/\text{Fe}]$  and  $[\text{Zn}/\text{Fe}]$ , reaching up to 0.5/0.7 dex for the latter ratio.

These usually poorly explored abundance ratios are, thus, able to distinguish stars formed in low star formation rate environments, like those of dwarf galaxies, in the metal-rich regime, where more commonly investigated abundance ratios (like the explosive  $\alpha$ -elements or neutron capture elements) lose their sensitivity as a proxy of different stellar birth places.

In this Letter we apply the tools proposed in Minelli et al. (2021) for chemical tagging to four metal-rich GCs, namely NGC 5927, NGC 6496, NGC 6388, and NGC 6441. These GCs have similar metallicities ( $[\text{Fe}/\text{H}] \sim -0.5$  dex) and they are thus located in the metallicity range where the iron-peak element abundance ratios should exhibit the largest discrepancy in case they have a different origin (Minelli et al. 2021). According to their dynamical properties, the first two have been clearly identified as in situ clusters (Massari et al. 2019). On the other hand, the other two seem to share an accreted origin, but their orbital properties make their classification more uncertain (see Massari et al. 2019; Kruijssen et al. 2020). These two clusters are usually associated with each other, in particular, because they exhibit extended blue horizontal branches (Rich et al. 1997), despite of their high metallicity, suggesting a high He content (Bellini et al. 2013).

## 2. Spectroscopic Data Sets

All the spectra have been acquired with the multi-object spectrograph UVES-FLAMES (Pasquini et al. 2002) mounted at

\* Based on observations collected at the ESO-VLT under programs 073.D-0211, 079.B-0721, and 193.D-0232.

the Very Large Telescope of ESO, using the grating 580 Red Arm CD#3, which provides a spectral resolution of  $R = 47,000$  and a spectral coverage between 4800 and 6800 Å. They have been reduced with the dedicated ESO pipelines,<sup>4</sup> including bias subtraction, flat-fielding, wavelength calibration, spectral extraction, and order merging. For each individual spectrum, the sky background has been subtracted, using the spectra obtained observing empty sky regions.

Considering the high luminosity/low temperature and high metallicity of the observed stars, we check for the presence of TiO molecular bands that can affect the derived chemical abundances and we exclude the contaminated spectra.

The targets of our analysis are four GCs. Their data were collected as follows:

1. *NGC 5927*—NGC 5927 is a disk MW GC (according to the classification adopted by Massari et al. 2019, disk clusters have the maximum height from the disk  $Z_{\max} < 5$  kpc and the orbital circularity  $\text{circ} < 0.5$ ). It has a metallicity of  $[\text{Fe}/\text{H}] = -0.47 \pm 0.02$  dex (Mura-Guzmán et al. 2018) and a mass of  $2.75 \pm 0.02 \times 10^5 M_{\odot}$  (the value is taken from the current latest version of the GC database by Holger Baumgardt, see Baumgardt & Hilker 2018). The data set for this GC is composed of five red giant branch (RGB) stars, observed under the ESO-VLT program 079.B-0721 (PI: Feltzing).
2. *NGC 6441*—This cluster has a metallicity of  $[\text{Fe}/\text{H}] = -0.39 \text{ dex} \pm 0.04$  (Gratton et al. 2006), a mass of  $1.32 \pm 0.01 \times 10^6 M_{\odot}$  (Baumgardt & Hilker 2018) and despite its orbit currently placing it in the Galactic Bulge, it likely has an accreted origin according to Massari et al. (2019). Among the four members identified by Gratton et al. (2006), we include in our analysis only the two giant stars observed under the ESO-VLT program: 073.D-0211 (PI: Carretta), whose spectra are not contaminated by TiO molecular bands.
3. *NGC 6388*—This cluster has a similar orbit compared to that of NGC 6441, yet Massari et al. (2019) classify it as an in situ Bulge GC (these authors define as bulge clusters those placed on highly bound orbits, with apocenter  $\text{apo} < 3.5$  kpc). It has a mean metallicity of  $[\text{Fe}/\text{H}] = -0.44 \pm 0.01$  dex (Carretta et al. 2007) and a mass of  $1.25 \pm 0.01 \times 10^6 M_{\odot}$  (Baumgardt & Hilker 2018). Among NGC 6388 stars observed under the ESO-VLT program: 073.D-0211 (PI: Carretta), we analyzed the four giants that are cluster members according to their radial velocity (Carretta et al. 2007) and whose spectra were not contaminated by TiO molecular bands.
4. *NGC 6496*—Just like NGC 5927, NGC 6496 is a disk MW GC. It has a metallicity of  $[\text{Fe}/\text{H}] = -0.46 \pm 0.07$  dex derived from low-resolution spectra (Carretta et al. 2009) and a mass of  $6.89 \pm 0.73 \times 10^4 M_{\odot}$  (Baumgardt & Hilker 2018). This data set includes five RGB stars belonging to this GC observed in the contest of the ESO-MIKiS survey (Ferraro et al. 2018), Large Programme 193.D-0232 (PI: Ferraro). The member stars are selected according to their radial velocity.

The elements we focus on in our investigation are generally not affected by the chemical peculiarities associated with the so-called phenomenon of multi-populations in GCs

(Bastian & Lardo 2018). The only possible exception is Sc, which shows possible variations in massive GCs (Carretta & Bragaglia 2021). NGC6441 and NGC6388 are indeed massive, but they do not show Sc variations according to the quoted analysis.

### 3. Analysis

The four target GCs are characterized by large values of color excess and differential reddening that make the atmospheric parameters of individual stars uncertain when derived from the photometry. Thanks to the large number of Fe I lines available in the UVES spectra, effective temperatures ( $T_{\text{eff}}$ ) can be easily derived by imposing the excitation equilibrium. As discussed by Mucciarelli & Bonifacio (2020), for metal-rich giant stars spectroscopic temperatures are consistent with the photometric temperatures and the method can be adopted safely (at variance with the metal-poor stars where the spectroscopic temperatures are biased and systematically underestimated, as shown in Figure 9 of Mucciarelli & Bonifacio 2020).

The surface gravity ( $\log g$ ) is derived by using theoretical isochrones computed with the Dartmouth Stellar Evolution Database (Dotter et al. 2008), adopting for each GC an isochrone with appropriate age (Forbes & Bridges 2010) and chemical mixture (we started with the literature value of  $[\text{Fe}/\text{H}]$  and  $[\alpha/\text{Fe}]$ , adapting in each interaction their value to the results of our analysis).

Finally, the microturbulent velocities ( $\xi$ ) of the stars are derived spectroscopically, by minimizing the slope between the abundances from Fe I lines and the reduced equivalent widths.

Abundances of Si, Ca, Ti, and Fe have been derived from the measured equivalent widths (EWs) of unblended lines using the code GALA (Mucciarelli et al. 2013). The EWs have been measured with DAOSPEC (Stetson & Pancino 2008) through the wrapper 4DAO (Mucciarelli 2013). A line-by-line inspection has been performed in order to check the continuum location and the best-fit for each individual line.

The chemical abundances for the species for which only blended lines (Sc, V, Ba, La, and Eu) or transitions located in noisy/complex spectral regions (Zn) are available, have been derived with our own code SALVADOR that performs a  $\chi^2$ -minimization between the observed line and a grid of suitable synthetic spectra calculated on the fly using the code SYNTHÉ (Kurucz 2005).

We exclude from our analysis those elements (O, Na, Mg, and Al) involved in the multiple population phenomenon (Bastian & Lardo 2018).

The procedure to select the lines used to derive the chemical abundances of the involved elements is described in Minelli et al. (2021). Atomic data for the selected lines are from the Kurucz/Castelli database, with more recent or more accurate data for some specific transition (see Mucciarelli et al. 2017, for additional references related to Fe, Si, Ca, Ti, Ba, and Eu lines). Atomic data for Sc and V lines are from MFW e NBS (Wiese & Fuhr 1975; Martin et al. 1988). For the Zn line at 4810 Å we adopt the oscillator strength by Roederer & Lawler (2012). Data for the La line at 6390 Å are from Lawler et al. (2001). Solar reference abundances are from Grevesse & Sauval (1998), for consistency with Minelli et al. (2021).

Errors in each abundance ratio have been calculated following the procedure described by Minelli et al. (2021) and propagating the uncertainties in astrophysical parameters into the chemical abundances.

<sup>4</sup> <http://www.eso.org/sci/software/pipelines/>

**Table 1**  
Atmospheric Parameters, Chemical Abundance Ratios, and Corresponding Uncertainty for the Individual Target Stars

star	$T$	$\log g$	$\xi$	[Fe/H]	err	[Si/Fe]	err	[Ca/Fe]	err	[Ti/Fe]	err	[Sc/Fe]	err	[V/Fe]	err	[Zn/Fe]	err	[Ba/Fe]	err	[La/Fe]	err	[Eu/Fe]	err
NGC 5927																							
5,039,161	4400	1.97	1.40	-0.42	0.04	+0.19	0.06	+0.10	0.08	+0.23	0.06	+0.28	0.05	+0.16	0.11	+0.07	0.07	+0.05	0.05	+0.08	0.06	+0.41	0.04
5,039,423	4550	2.25	1.60	-0.47	0.05	+0.19	0.06	+0.06	0.07	+0.22	0.06	+0.32	0.05	+0.19	0.09	+0.22	0.09	+0.02	0.07	+0.22	0.04	+0.48	0.04
5,040,219	4550	2.25	1.30	-0.51	0.04	+0.16	0.04	+0.10	0.06	+0.29	0.04	+0.36	0.04	+0.24	0.07	+0.32	0.07	+0.17	0.05	+0.28	0.04	+0.56	0.04
5,040,282	4500	2.16	1.20	-0.44	0.04	+0.13	0.05	+0.20	0.06	+0.24	0.05	+0.33	0.04	+0.21	0.08	+0.40	0.07	+0.04	0.04	+0.24	0.04	+0.46	0.04
5,041,223	4500	2.16	1.40	-0.47	0.05	+0.17	0.05	+0.07	0.07	+0.25	0.05	+0.38	0.05	+0.23	0.07	+0.30	0.07	+0.11	0.07	+0.24	0.04	+0.38	0.04
NGC 6388																							
77,599	4100	1.33	1.60	-0.49	0.09	+0.39	0.09	+0.07	0.12	+0.22	0.13	+0.01	0.05	-0.19	0.15	-0.07	0.09	-0.03	0.09	+0.16	0.05	+0.43	0.04
83,168	4150	1.42	1.50	-0.46	0.07	+0.19	0.09	-0.00	0.13	+0.15	0.13	+0.05	0.06	-0.17	0.17	-0.21	0.08	+0.08	0.08	+0.12	0.10	+0.31	0.04
108,895	4000	1.16	1.50	-0.51	0.03	+0.19	0.05	-0.04	0.09	+0.06	0.07	+0.02	0.04	-0.33	0.11	-0.12	0.06	+0.10	0.05	+0.07	0.04	+0.33	0.03
110,677	4000	1.16	1.50	-0.50	0.03	+0.19	0.06	-0.10	0.11	+0.03	0.10	-0.03	0.07	-0.32	0.13	-0.07	0.10	+0.05	0.06	+0.12	0.07	+0.27	0.04
NGC 6441																							
7,004,463	3950	1.07	1.40	-0.48	0.03	+0.30	0.06	+0.16	0.11	+0.18	0.07	+0.11	0.10	-0.29	0.10	-0.38	0.14	+0.02	0.05	-0.03	0.05	+0.38	0.05
7,004,487	4050	1.24	1.20	-0.59	0.04	+0.23	0.09	+0.11	0.09	+0.18	0.10	-0.05	0.09	-0.34	0.12	-0.60	0.14	-0.13	0.07	+0.04	0.07	+0.30	0.06
NGC 6496																							
14	4150	1.48	1.30	-0.61	0.03	+0.31	0.04	+0.27	0.05	+0.34	0.05	+0.38	0.04	+0.25	0.12	+0.48	0.17	+0.27	0.06	+0.29	0.06	+0.52	0.05
17	4150	1.48	1.30	-0.64	0.03	+0.29	0.05	+0.20	0.07	+0.31	0.06	+0.41	0.05	+0.19	0.15	+0.21	0.17	+0.29	0.06	+0.32	0.06	+0.48	0.05
18	4150	1.48	1.40	-0.68	0.03	+0.27	0.05	+0.24	0.06	+0.29	0.05	+0.36	0.10	+0.17	0.14	+0.40	0.18	+0.08	0.11	+0.28	0.06	+0.48	0.06
26	4400	1.94	1.40	-0.60	0.04	+0.30	0.04	+0.05	0.04	+0.19	0.06	+0.36	0.05	+0.10	0.07	+0.12	0.09	+0.21	0.05	+0.20	0.05	+0.55	0.04
159	4100	1.39	1.20	-0.65	0.03	+0.28	0.04	+0.23	0.05	+0.29	0.05	+0.37	0.04	+0.16	0.12	+0.23	0.09	+0.26	0.05	+0.21	0.04	+0.50	0.03

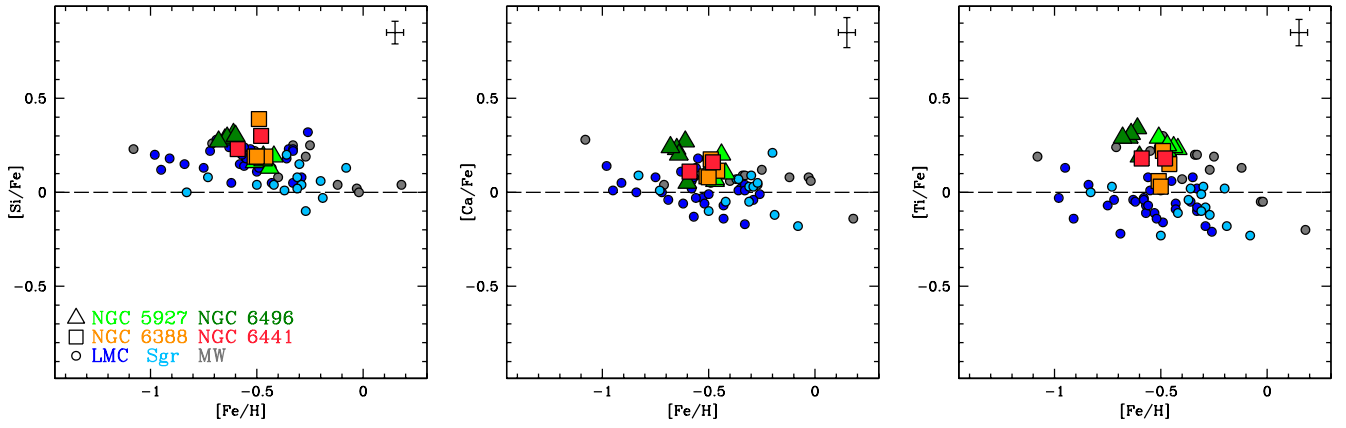


**Figure 1.** Behavior of the  $\alpha$  elements [Si/Fe], [Ca/Fe], and [Ti/Fe] abundance ratios (from left to right, respectively) as a function of [Fe/H] for NGC 5927 (light green triangles), NGC 6388 (orange squares), NGC 6441 (red squares), NGC 6496 (dark green triangles), with LMC (blue dots), Sgr (light blue dots), and MW (gray dots) as reference.

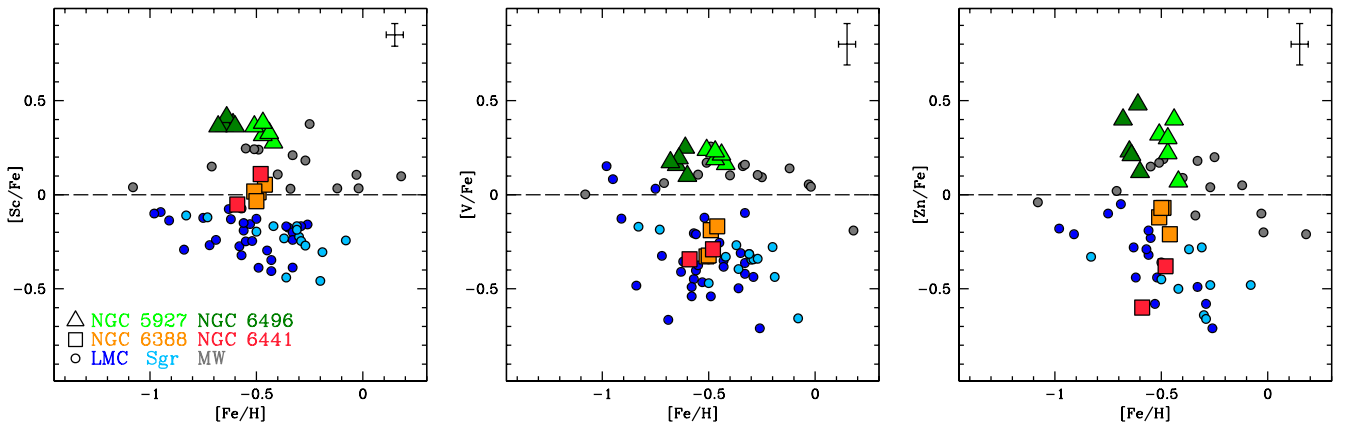


**Figure 2.** Behavior of the iron-peak elements [Sc/Fe], [V/Fe], and [Zn/Fe] abundance ratios (from left to right, respectively) as a function of [Fe/H] for NGC 5927, NGC 6388, NGC 6441, NGC 6496, LMC, Sgr, and MW (same symbols as Figure 1).

**Table 2**  
Mean Abundance Ratios (and Corresponding Standard Deviation) for the Four Target Clusters

Element	NGC 5927		NGC 6388		NGC 6441		NGC 6496	
	Mean	$\sigma$	Mean	$\sigma$	Mean	$\sigma$	Mean	$\sigma$
[Fe/H]	-0.46	0.03	-0.49	0.02	-0.54	0.08	-0.64	0.03
[Si/Fe]	+0.17	0.02	+0.24	0.10	+0.27	0.05	+0.29	0.02
[Ca/Fe]	+0.11	0.06	+0.11	0.04	+0.14	0.04	+0.20	0.09
[Ti/Fe]	+0.25	0.03	+0.12	0.09	+0.18	0.00	+0.28	0.06
[Sc/Fe]	+0.33	0.04	+0.01	0.04	+0.03	0.11	+0.38	0.02
[V/Fe]	+0.21	0.03	-0.25	0.09	-0.32	0.04	+0.17	0.05
[Zn/Fe]	+0.26	0.12	-0.12	0.07	-0.49	0.16	+0.29	0.15
[Ba/Fe]	+0.07	0.06	+0.05	0.05	-0.05	0.10	+0.22	0.09
[La/Fe]	+0.21	0.08	+0.12	0.04	+0.01	0.05	+0.26	0.05
[Eu/Fe]	+0.46	0.07	+0.34	0.07	+0.34	0.06	+0.51	0.03

#### 4. Results and Discussion

The objective of our analysis is to investigate whether the four GCs, all with a similar [Fe/H]  $\sim -0.5$  dex, show any differences in their elemental abundances, with particular focus on the iron-peak elements that have proven to be effective in distinguishing accretion from in situ stars in this metal-rich regime. To do so, we homogeneously analyze high-resolution spectra of RGB stars belonging to these Galactic GCs. The

abundances measured in individual stars, together with their atmospheric parameters, are listed in Table 1, and the mean abundance ratios of the GCs for the analyzed species are reported in Table 2.

Figures 1–3 show the measured abundance ratios for  $\alpha$ -elements, iron-peak elements, and neutron capture elements, as a function of [Fe/H] for the stars analyzed in the four target clusters. We can immediately appreciate that the  $\alpha$ -elements Si and Ca show similar abundance ratios in all four GCs. Slow

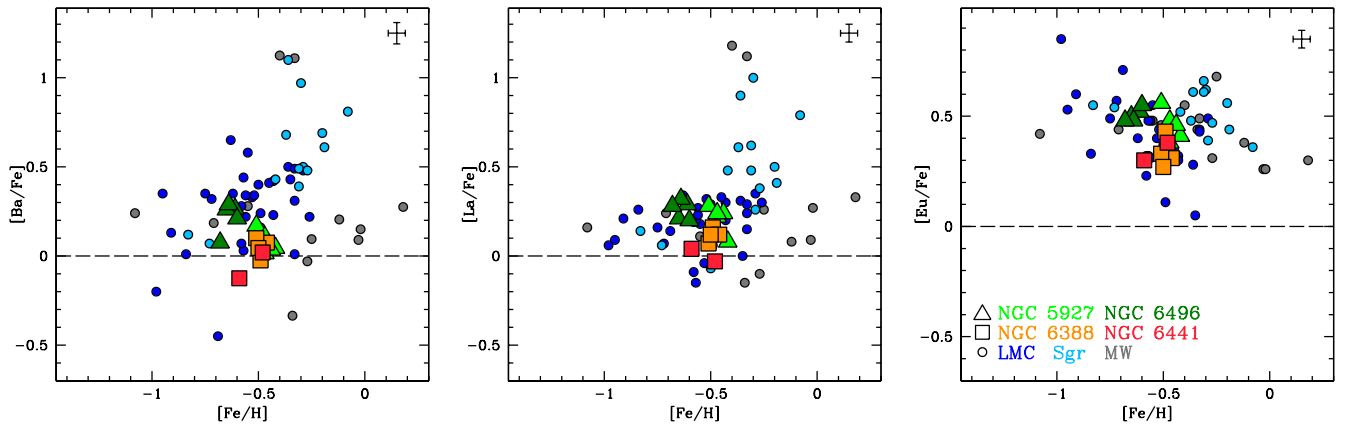


**Figure 3.** Behavior of the neutron capture elements [Ba/Fe], [La/Fe], and [Eu/Fe] abundance ratios (from left to right, respectively) as a function of [Fe/H] for NGC 5927, NGC 6388, NGC 6441, NGC 6496, LMC, Sgr, and MW (same symbols as Figure 1).

(La and Ba) and rapid (Eu) neutron capture elements, in addition to Ti, show a marginal discrepancy, with NGC 6388 and NGC 6441 being underabundant compared to NGC 5927 and NGC 6496 at the 1–2 $\sigma$  level from the comparison between the mean abundance values and their standard deviation. On the other hand, a stark difference (at a significance level always larger than 3 $\sigma$ , up to  $\sim 10\sigma$ ) is found when considering the abundances of Sc, V, and Zn. In particular, NGC 6388 and NGC 6441 have abundance ratios for these iron-peak elements significantly lower than those measured in NGC 5927 and NGC 6496. We stress that these differences cannot be attributed to some systematics in the chemical analysis because the assumptions in the analysis of all the GCs are the same (i.e., the reference solar abundances, the atomic data, the model atmospheres, and the method to derive the atmospheric parameters), and we analyze stars of similar spectral type. Therefore, the origin of the different [Sc/Fe], [V/Fe], and [Zn/Fe] chemical abundance ratios must be intrinsic, due to a real difference in the chemical enrichment path followed by the gas from which the two pairs of clusters formed.

Interesting enough, the differences in these abundance ratios for the two pairs of GC, match well those measured by Minelli et al. (2021) between LMC/Sgr and MW field stars of similar metallicity (overplotted in Figures 1–3 as small filled circles). In particular, NGC 6388 and NGC 6441 exhibit [Sc/Fe], [V/Fe], and [Zn/Fe] abundances similar to those measured in LMC/Sgr stars, while NGC 5927 and NGC 6496 have abundances similar to those of MW stars. We remark that according to many results in the literature (Bensby et al. 2003, 2017; Battistini & Bensby 2015; Duong et al. 2019; Griffith et al. 2021; Lucey et al. 2021) the iron-peak element abundance ratios of MW disk and bulge stars are consistent with each other. All these works found abundance values similar to those of NGC 5927 and NGC 6496, but different from those of NGC 6388 and NGC 6441. Minelli et al. (2021) interpret the low abundance ratios in LMC/Sgr stars in terms of a lower contribution from massive stars to the chemical enrichment, compared to that experienced by the MW. The reason for this would be that these elements are mainly produced by hypernovae, Type II supernovae, or electron-capture supernovae with high-mass stellar progenitors. In particular, hypernovae (associated with stars more massive than  $\sim 25\text{--}30 M_{\odot}$ ) would produce most Zn, without a sizeable contribution from type Ia supernovae (Romano et al. 2010; Kobayashi et al. 2020). Hence, the ratio [Zn/Fe] is expected to

decrease significantly in galaxies with a low star formation rate, where the contribution by massive stars is reduced (Yan et al. 2017; Jeřábková et al. 2018).

In light of this finding, it is natural to conclude that both NGC 6388 and NGC 6441 should have formed from a gas poorly enriched by massive stars, at odds with what was observed for the other two investigated clusters. Thus, the analysis presented here offers an independent confirmation that NGC 5927 and NGC 6496 formed in situ, as already suggested by the kinematics (Massari et al. 2019), and identifies NGC 6388 and NGC 6441 as likely formed in an external environment, characterized by chemical enrichment histories influenced by a low star formation rate, and only later accreted by the MW. It is interesting to note that of the two clusters identified here as accreted, the kinematics analysis by Massari et al. (2019) indicated only NGC 6441 as an accreted cluster associated with the Kraken merger event (see Kruijssen et al. 2020), while an unclear origin was indicated for NGC 6388. Therefore, in light of the similar chemical abundances of the two GCs, NGC 6388 should have formed from the same progenitor of NGC 6441 or at least from a system with a chemical enrichment history similar to that of Kraken.

In summary, the use of the iron-peak elemental abundances proposed by Minelli et al. (2021) has allowed us to shed light on the origin of the metal-rich GCs, NGC 6388 and NGC 6441, indicating also NGC 6388 as a possible accreted cluster from a progenitor similar to Kraken in spite of the fact that its dynamical properties were not sufficient to unambiguously determine its birth place.

Unlike Zn, whose nucleosynthesis in stars is pretty well understood (see previous paragraphs), the detailed nucleosynthetic paths leading to the stellar production of Sc and V still deserve investigation (see Cowan et al. 2020; Kobayashi et al. 2020 for recent reappraisals from the observational and theoretical point of view, respectively). Notably, different initial conditions of exploding white dwarfs leading to type Ia supernovae may result in very different V yields (e.g., Shen et al. 2018; Leung & Nomoto 2020) with sizable consequences on the predictions of chemical evolution models (Palla 2021) that have yet to be fully explored. Our results clearly highlight the importance of Sc, V, and Zn as chemical taggers and will hopefully inspire further theoretical work.

We thank the referee, Chris Sneden, for his useful comments and suggestions. This research is funded by the project “Light-

on-Dark”, granted by the Italian MIUR through contract PRIN-2017K7REXT.

### ORCID iDs

A. Minelli  <https://orcid.org/0000-0002-5304-9866>  
 A. Mucciarelli  <https://orcid.org/0000-0001-9158-8580>  
 D. Massari  <https://orcid.org/0000-0001-8892-4301>  
 M. Bellazzini  <https://orcid.org/0000-0001-8200-810X>  
 D. Romano  <https://orcid.org/0000-0002-0845-6171>  
 F. R. Ferraro  <https://orcid.org/0000-0002-2165-8528>

### References

- Bastian, N., & Lardo, C. 2018, *ARA&A*, 56, 83  
 Battistini, C., & Bensby, T. 2015, *A&A*, 577, A9  
 Baumgardt, H., & Hilker, M. 2018, *MNRAS*, 478, 1520  
 Bellini, A., Piotto, G., Milone, A. P., et al. 2013, *ApJ*, 765, 32  
 Bensby, T., Feltzing, S., Gould, A., et al. 2017, *A&A*, 605, A89  
 Bensby, T., Feltzing, S., & Lundström, I. 2003, *A&A*, 410, 527  
 Carretta, E., & Bragaglia, A. 2021, *A&A*, 646, A9  
 Carretta, E., Bragaglia, A., Gratton, R., et al. 2009, *A&A*, 508, 695  
 Carretta, E., Bragaglia, A., Gratton, R. G., et al. 2007, *A&A*, 464, 967  
 Cowan, J. J., Sneden, C., Roederer, I. U., et al. 2020, *ApJ*, 890, 119  
 Dotter, A., Chaboyer, B., Jevremović, D., et al. 2008, *ApJS*, 178, 89  
 Duong, L., Asplund, M., Nataf, D. M., et al. 2019, *MNRAS*, 486, 5349  
 Fernández-Alvar, E., Carigi, L., Schuster, W. J., et al. 2018, *ApJ*, 852, 50  
 Ferraro, F. R., Mucciarelli, A., Lanzoni, B., et al. 2018, *ApJ*, 860, 50  
 Forbes, D. A. 2020, *MNRAS*, 493, 847  
 Forbes, D. A., & Bridges, T. 2010, *MNRAS*, 404, 1203  
 Freeman, K., & Bland-Hawthorn, J. 2002, *ARA&A*, 40, 487  
 Gratton, R. G., Lucatello, S., Bragaglia, A., et al. 2006, *A&A*, 455, 271  
 Grevesse, N., & Sauval, A. J. 1998, *SSRv*, 85, 161  
 Griffith, E., Weinberg, D. H., Johnson, J. A., et al. 2021, *ApJ*, 909, 77  
 Helmi, A. 2020, *ARA&A*, 58, 205  
 Helmi, A., Babusiaux, C., Koppelman, H. H., et al. 2018, *Natur*, 563, 85  
 Jeřábková, T., Hasani Zonoozi, A., Kroupa, P., et al. 2018, *A&A*, 620, A39  
 Kobayashi, C., Karakas, A. I., & Lugaro, M. 2020, *ApJ*, 900, 179  
 Kruijssen, J. M. D., Pfeffer, J. L., Chevance, M., et al. 2020, *MNRAS*, 498, 2472  
 Kruijssen, J. M. D., Pfeffer, J. L., Reina-Campos, M., et al. 2019, *MNRAS*, 486, 3180  
 Kurucz, R. L. 2005, *MSAIS*, 8, 14  
 Lawler, J. E., Bonvallet, G., & Sneden, C. 2001, *ApJ*, 556, 452  
 Leung, S.-C., & Nomoto, K. 2020, *ApJ*, 900, 54  
 Lucey, M., Hawkins, K., Ness, M., et al. 2021, arXiv:2107.02793  
 Martin, G. A., Fuhr, J. R., & Wiese, W. L. 1988, Atomic Transition Probabilities. Scandium Through Manganese (New York: AIP)  
 Massari, D., Koppelman, H. H., & Helmi, A. 2019, *A&A*, 630, L4  
 Matteucci, F., & Brocato, E. 1990, *ApJ*, 365, 539  
 Minelli, A., Mucciarelli, A., Romano, D., et al. 2021, *ApJ*, 910, 114  
 Mucciarelli, A. 2013, arXiv:1311.1403  
 Mucciarelli, A., & Bonifacio, P. 2020, *A&A*, 640, A87  
 Mucciarelli, A., Monaco, L., Bonifacio, P., et al. 2017, *A&A*, 603, L7  
 Mucciarelli, A., Pancino, E., Lovisi, L., et al. 2013, *ApJ*, 766, 78  
 Mura-Guzmán, A., Villanova, S., Muñoz, C., et al. 2018, *MNRAS*, 474, 4541  
 Palla, M. 2021, *MNRAS*, 503, 3216  
 Pasquini, L., Avila, G., Blecha, A., et al. 2002, *Msngr*, 110, 1  
 Rich, R. M., Sosin, C., Djorgovski, S. G., et al. 1997, *ApJL*, 484, L25  
 Roederer, I. U., & Lawler, J. E. 2012, *ApJ*, 750, 76  
 Romano, D., Karakas, A. I., Tosi, M., et al. 2010, *A&A*, 522, A32  
 Shen, K. J., Kasen, D., Miles, B. J., et al. 2018, *ApJ*, 854, 52  
 Stetson, P. B., & Pancino, E. 2008, *PASP*, 120, 1332  
 Tolstoy, E., Hill, V., & Tosi, M. 2009, *ARA&A*, 47, 371  
 White, S. D. M., & Rees, M. J. 1978, *MNRAS*, 183, 341  
 Wiese, W. L., & Fuhr, J. R. 1975, *JPCRD*, 4, 263  
 Yan, Z., Jerabkova, T., & Kroupa, P. 2017, *A&A*, 607, A126